J. Fluid Mech. (2025), *vol.* 1022, R3, doi:10.1017/jfm.2025.10799



Induced periodicity in wakes

Ingrid Neunaber[1,2], **Srikar Yadala**[1] and **R. Jason Hearst**[1]

[1]Department of Energy & Process Engineering, Norwegian University of Science & Technology, NO-7491, Trondheim, Norway

[2]FLOW, Department of Engineering Mechanics, KTH Royal Institute of Technology, SE-114 28, Stockholm, Sweden

Corresponding author: Ingrid Neunaber, neunaber@kth.se

(Received 13 August 2025; revised 25 September 2025; accepted 28 September 2025)

Wakes and the dynamic interactions of multiple wakes have been a focal point of numerous research endeavours. Traditionally, wake interaction studies have focused on wakes produced by similar bodies. In contrast, the present study positions a non-shedding porous disc adjacent to periodically shedding solid discs of varying diameters and dimensional shedding frequencies. Using hot-wire measurements, we explore the intriguing interaction between these wakes. Remarkably, our findings reveal that the wake of the non-shedding disc acquires oscillations from the wake of the shedding disc, irrespective of their distinct frequencies. We demonstrate high receptivity of the porous disc's wake and connect our findings to real-life applications.

Key words: wakes, vortex shedding, vortex streets

1. Introduction

Wakes, the velocity defect region behind a body in a flow, are typically investigated in isolation (e.g. Castro 1971; Nedić *et al.* 2013; Vinnes *et al.* 2022; Bourhis & Buxton 2024; Cicolin *et al.* 2024; Steiros *et al.* 2025) and sometimes in situations where two identical bodies produce identical wakes that interact (e.g. Wong *et al.* 2014; Zhou & Mahbub Alam 2016; Maus, Peinke & Hölling 2022; Obligado, Klein & Vassilicos 2022; Berstad, Hearst & Neunaber 2025). In contrast, there are many applications where wakes with different properties, such as vortex shedding or the lack thereof, can interact, for example in urban environments (Hertwig *et al.* 2019), bridges (Song *et al.* 2024) or wind farms (Martínez-Tossas *et al.* 2022), where wakes of floating turbines have been shown to exhibit particularly complex dynamics (e.g. Kleine *et al.* 2022; Messmer, Hölling & Peinke

© The Author(s), 2025. Published by Cambridge University Press. This is an Open Access article, distributed under the terms of the Creative Commons Attribution licence (https://creativecommons.org/licenses/by/4.0/), which permits unrestricted re-use, distribution and reproduction, provided the original article is properly cited.

https://doi.org/10.1017/jfm.2025.10799 Published online by Cambridge University Press

2024). Herein, we investigate the situation where a 'dead' wake with no periodic signature interacts with another turbulent flow (another wake) with a strong periodic signature and demonstrate some surprising phenomena.

Significant literature exists for the case of side-by-side cylinders where the typical objective is to investigate the interaction of the von Kármán vortex streets (Wong *et al.* 2014; Zhou & Mahbub Alam 2016). From the interaction of vortex streets from cylinders of different sizes, it is well known that secondary peaks can occur at the sum and difference of their two individual shedding frequencies, e.g. Baj & Buxton (2017) and Cicolin *et al.* (2021).

The interaction of axisymmetric wakes is, in contrast, typically investigated from either a wind energy perspective ('how do velocity deficits add up in a wind farm?', e.g. Porté-Agel *et al.* (2020), Bastankhah *et al.* (2021) and Hegazy *et al.* (2022)) or a turbulence perspective ('how does the turbulence between two wakes interact?', e.g. Scott *et al.* (2020), Maus *et al.* (2022), Obligado *et al.* (2022) and Berstad *et al.* (2025)). Recently, Obligado *et al.* (2022) illustrated the interaction of axisymmetric wakes from two different types of plates – fractal and square solid plates – at varying spanwise spacings. They discuss three downstream regions in the interaction and turbulence evolution process, providing evidence of non-equilibrium turbulence and indicating complex turbulence interactions. While these plates exhibit vortex shedding, cf. Nedić *et al.* (2013), this was not a focus of that study. In a similar manner, Berstad *et al.* (2025) investigated the interaction of axisymmetric wakes from two different types of porous discs at varying spanwise spacings. By means of the energy spectrum and the Castaing parameter, they identified three consecutive turbulence evolution stages in the merging process of the wakes that occur independently of the disc type and spacing.

Here, we combine solid discs with different diameters, known to shed (e.g. Miau *et al.* 1997), with a porous disc that is known to be modifiable such that it does not exhibit vortex shedding (e.g. Castro 1971; Vinnes *et al.* 2022; Bourhis & Buxton 2024; Cicolin *et al.* 2024; Steiros *et al.* 2025) in a side-by-side configuration. We experimentally investigate the interaction of these wakes to shed light on the interaction of dissimilar wakes which is of interest for flows in and around urban environments, bridges or wind farms (e.g. Hertwig *et al.* 2019; Martínez-Tossas *et al.* 2022; Song *et al.* 2024). The data are analysed in terms of mean velocity, turbulence intensity and power spectral density. Linear stability analysis is performed in addition for the wakes of the single discs.

2. Methodology

The experiments were conducted in the Large Scale Wind Tunnel at the Norwegian University of Science and Technology in Trondheim, Norway. The tunnel has dimensions of $11.1\,\mathrm{m} \times 1.8\,\mathrm{m} \times 2.71\,\mathrm{m}$ (length $\times$ height $\times$ width). To keep the pressure gradient in the streamwise direction approximately zero, the height of the roof is gradually adjusted to 1.91 m to compensate for boundary layer growth. The inlet velocity, U_∞, was approximately $10\,\mathrm{m\,s^{-1}}$, and the turbulence intensity, u'/U, of the free-stream was below 0.3 %, where u' is the standard deviation of the velocity and U denotes its local mean value. Velocity measurements were obtained using one-component hot-wire anemometry where an automated traversing system moved the single wire through the wind tunnel. The measurements were performed with a sampling frequency of $f_s = 75047\,\mathrm{Hz}$ for $t = 180\,\mathrm{s}$, and a hardware low-pass filter was set at $f_{lp} = 30\,\mathrm{kHz}$. The hot-wire was calibrated approximately every 4–5 h, and temperature correction was applied (Hultmark & Smits 2010). A weighted average of the calibrations was used for the measurements taken in between the calibrations. Applying the method of Benedict & Gould (1996), the maximum

https://doi.org/10.1017/jfm.2025.10799 Published online by Cambridge University Press

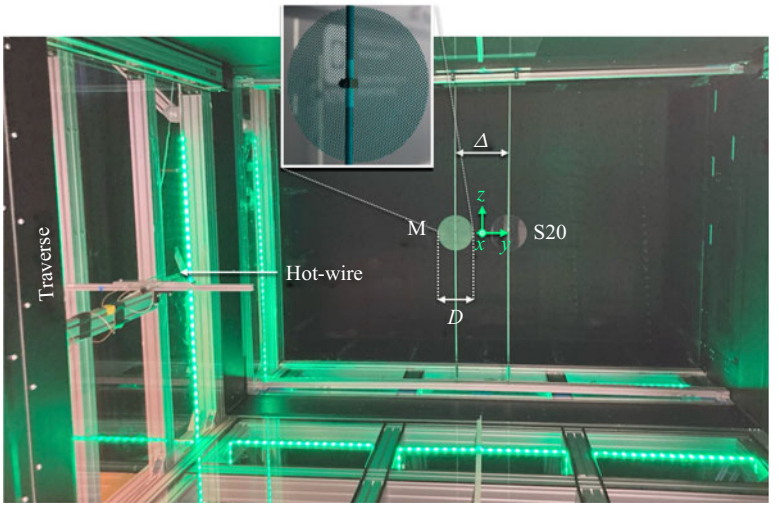


Figure 1. Photograph of the wind tunnel set-up with the mesh disc M and the solid disc S20 with a spacing of Δ. A magnified photograph of the M disc is shown in the inset. The coordinate system is indicated; the mean flow is in the x-direction, which is out of the page. The hot-wire and traverse are marked.

random error of the mean velocity is 1.1 % or less and the maximum random error of the turbulence intensity is 1 % or less. Mean velocities are converged within ± 0.5 % after 60 s; standard deviations are converged within ± 1.0 % after 120 s or earlier if the turbulence is sufficiently developed at the respective position, if not (e.g. at the wake borders), the convergence is within ± 2.0 %. Note that, as the shear layers are more difficult to capture than the wake cores, convergence and uncertainty are better in regions that are not subject to high intensity intermittent flow.

As noted above, measurements were obtained downstream of two different types of discs in a side-by-side setting. The first is a uniform mesh disc, referred to as type M, with a blockage of 57 %, a thickness of nominally 1 mm and a diameter $D = 200$ mm. This specific disc has been used several times in the literature where it has been well characterised (Aubrun *et al.* 2019; Vinnes *et al.* 2022, 2023; Berstad *et al.* 2025; Hölling *et al.* 2025). The second disc was selected from an array of solid discs made from acrylic plates with a thickness of 5 mm. These are referred to as type S. Solid discs are also well characterised in the literature. Three diameters were investigated for the solid discs, $D_{S20} = 200$, $D_{S17} = 170$ and $D_{S10} = 100$ mm, and they are labelled S20, S17 and S10, respectively. The three investigated combinations are M-S20, M-S17 and M-S10. The spacing between the disc centres was $\Delta = 2D = 400$ mm for all cases, where, for side-by-side cylinders and flat plates, two vortex streets coupled in phase would be expected (Zhou & Mahbub Alam 2016; Dadmarzi *et al.* 2018). The diameter-based Reynolds number, $Re_D = U_\infty D/\nu$, where ν is the kinematic viscosity, is approximately 125 000 for a (fixed) diameter of $D = 200$ mm.

A photograph of both discs, their mounting and the coordinate system used here is shown in figure 1. The discs were fixed to metallic rods with a diameter of 10 mm, which were secured at the top and bottom of the wind tunnel using tensioning screws to prevent vibrations. Note that the shedding frequency of these rods is approximately 200 Hz, which is an order of magnitude higher than that of the solid discs, cf. § 3. The model solid blockage of two discs in the wind tunnel is 1.3 % for two discs with diameter D, and the blockage of the whole set-up, including the discs, rods and support structures is 6 %.

https://doi.org/10.1017/jfm.2025.10799 Published online by Cambridge University Press

Type	D_i/mm	δ/D_i	f_v/Hz	St
M	200	0.48	–	–
S20	200	1.2	7.5	0.146
S17	170	1.12	8.9	0.148
S10	100	1.16	15.4	0.150

Table 1. Diameters, integral wake widths, shedding frequencies and measured Strouhal numbers of the different discs at $8D_i$ downstream.

3. Individual wakes

The wakes generated by both this specific mesh disc (Aubrun *et al.* 2019; Vinnes *et al.* 2022, 2023; Hölling *et al.* 2025) and solid discs in general (e.g. Miau *et al.* 1997; Brown & Roshko 2012) have been well characterised in the literature. Nevertheless, before investigating the interaction of two side-by-side wakes, wakes of the employed single discs were characterised by measuring radial profiles $8D_i$ downstream in steps of $0.25D_i$ for $-2.5 \leqslant y/D_i \leqslant 2.5$. The respective diameters of the discs are denoted by D_i. The normalised mean velocity and turbulence intensity profiles are presented in figures 2(*a*) and 2(*b*). The profiles of the three solid discs collapse as expected. Contrarily, the profiles of the mesh disc wake exhibit a significantly stronger velocity deficit and turbulence intensity. This is in agreement with Vinnes *et al.* (2022, 2023), who demonstrated that the wake generated by the non-shedding M disc exhibits a slower turbulence build-up and velocity recovery than a shedding disc, resulting in a larger mean velocity deficit and higher turbulence intensity.

The modified constant eddy viscosity wake model (Cafiero, Obligado & Vassilicos 2020)

$$\frac{U_\infty - U(y/\delta)}{U_\infty - U_c} = a_1 \cdot e^{-a_2 \cdot (y/\delta)^2 - a_3 \cdot (y/\delta)^4 - a_4 \cdot (y/\delta)^6}, \tag{3.1}$$

was fit to the mean velocity profiles as shown in figure 2(*a*) (dashed lines). Here, a_1, a_2, a_3 and a_4 are fitting parameters, U_c is the velocity at the centreline of the respective discs and δ is the half-wake width, where $\delta^2 = (1/U_\infty - U_c)\int_0^\infty (U_\infty - U) r \mathrm{d}r$. The values for δ are reported in table 1. The width of the three solid discs' wakes is approximately $1.2D_i$, but that of the mesh disc is significantly thinner at $\approx 0.48D_i$. The profiles of the four tested discs align closely with this fit, highlighting the wake's predictable behaviour $8D_i$ downstream. It is noteworthy that the fitted values for a_3 and a_4 are very small. While these coefficients produce small modifications to reduce the error of the fits, (3.1) in fact reduces to a Gaussian distribution, $a_1 \cdot e^{-a_2 \cdot (y/\delta)^2}$, if $a_3 = a_4 = 0$; a Gaussian distribution is predominantly used in canonical literature to fit the wake's mean velocity profiles (e.g. Sato & Okada 1966).

The shedding frequencies of the various discs are deciphered by computing the energy spectra $E(f)$ of the streamwise velocity fluctuations in the shear layers (red markers in figures 2*a* and 2*b*) and are shown in figure 2(*c*). For the solid discs, distinct peaks attributed to vortex shedding can be identified, and the frequencies, f_v, and corresponding Strouhal numbers $St = D_i \cdot f_v / U_\infty \approx 0.15$, similar to those discussed in Miau *et al.* (1997), are noted in table 1. In agreement with Vinnes *et al.* (2022), there is no shedding peak in the wake of the mesh disc, which has been attributed to the missing recirculation region downstream of plates with blockage below approximately 75 % (Castro 1971; Cicolin *et al.* 2024).

https://doi.org/10.1017/jfm.2025.10799 Published online by Cambridge University Press

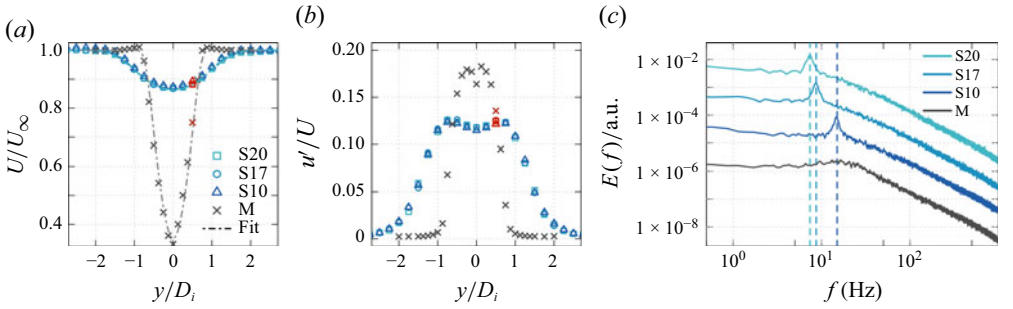


Figure 2. Single disc statistics at $8D_i$ downstream. (*a*) Normalised mean velocity profiles with fitted profiles; the red markers signify where the spectra are calculated. (*b*) Turbulence intensity profiles. Note, in (*a*) and (*b*) distinct curves for the solid disc cases are not visible because they collapse. (*c*) Spectra in the shear layers. For better visualisation, the spectra are shifted vertically.

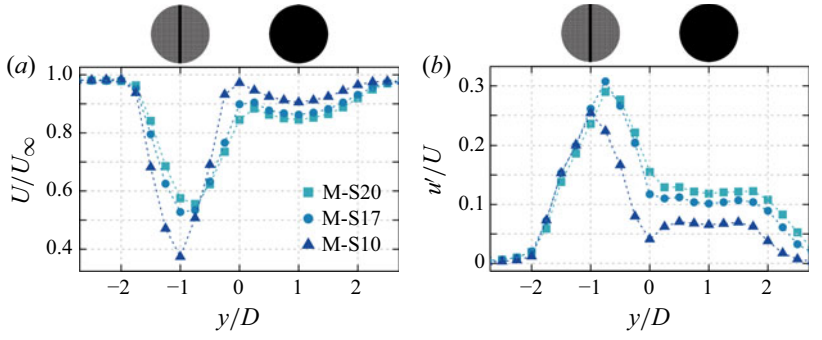


Figure 3. Spanwise profiles of (*a*) normalised mean velocity and (*b*) turbulence intensity for the three disc combinations M-S20, M-S17 and M-S10 measured at $8D$ downstream.

4. Phenomenological observations of wake interaction

Having characterised the single disc wakes, interactions of the wakes in the side-by-side disc configurations (M-S20, M-S17 and M-S10) are now investigated. For this, radial profiles were measured $8D$ downstream of the side-by-side discs in transverse steps of $0.25D$ for $-2.5 \leqslant y/D \leqslant 2.5$. Here, the M disc was centred at $y/D = 1$ while the solid discs were centred at $y/D = -1$. Figure 3 presents the spanwise profiles of the normalised mean velocity and the turbulence intensity for the three different configurations tested. In all cases, the wakes of the two discs interact. This can be inferred from the turbulence intensity level at the centreline exceeding the turbulence intensity of the inflow ($u'/U|_{y/D=0} > 0.3\,\%$). In addition, a larger mean velocity deficit and higher turbulence intensity are observed downstream of the mesh disc compared with the solid discs, which is consistent with the single wakes in figures 2(*a*) and 2(*b*) and Vinnes *et al.* (2022, 2023). Finally, we would like to note that the mean velocity deficit and turbulence intensity downstream of the solid discs increase with increasing disc diameter because, compared with the respective solid disc's diameter, the downstream position varies: measurements are taken at $x = 8D = 1600$ mm, which corresponds to $9.4D_{S17}$ or $16D_{S10}$ for S17 and S10, respectively, and as such, the smaller solid disc wakes are further evolved; note, the M disc always has a fixed diameter of $D = 200$ mm, which is why that value is used as a reference.

The spectrograms in figures 4(*a*), 4(*c*) and 4(*e*) show the spanwise pre-multiplied spectra $E(f) \cdot f$ for the three disc combinations at $8D$ downstream. The pre-multiplied spectrum

https://doi.org/10.1017/jfm.2025.10799 Published online by Cambridge University Press

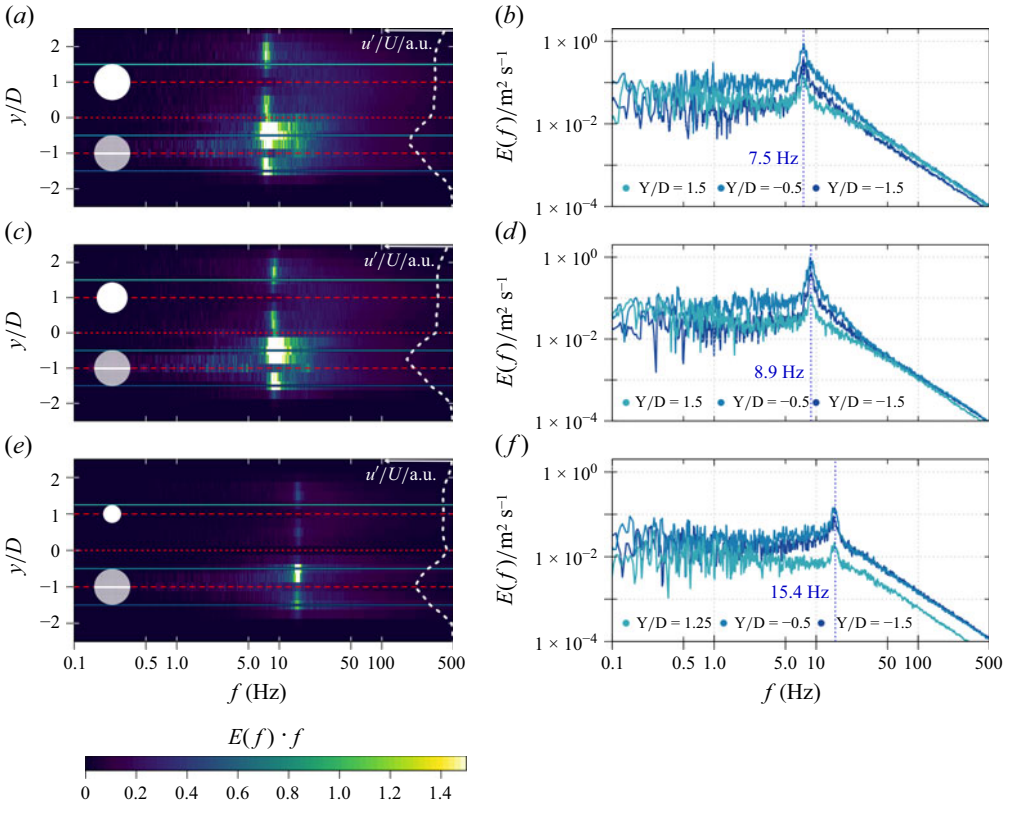


Figure 4. Spanwise pre-multiplied spectrograms of the three disc combinations (*a*) M-S20, (*c*) M-S17 and (*e*) M-S10 at $x/D = 8$. Red lines mark the wind tunnel centreline and the disc centrelines. The u'/U profiles are indicated by dashed white lines. Corresponding line spectra are plotted at selected spanwise positions in the shear layers for the three disc combinations (*b*) M-S20, (*d*) M-S17 and (*f*) M-S10. The positions are marked by lines of the same colour in the spectrograms.

shows the energy at a specific frequency, which helps to identify the most energetic frequencies in the contour plots. The shedding peaks of the solid discs are clearly visible downstream in their respective wakes and are at the same frequency as the single disc measurements. However, the wake downstream of the originally non-shedding mesh disc now exhibits a spectral peak at the respective shedding frequency of the solid disc in both shear layers. In fact, the peak is stronger downstream of the mesh disc than downstream of the originally shedding solid disc. To emphasise this, figures 4(*b*), 4(*d*) and 4(*f*) show the line spectra at both sides of the mesh disc and the spectrum at the outer side of the solid disc for the three cases. This indicates that the originally 'dead' wake now has a periodicity at the shedding frequency of the disc next to it. This periodicity is even stronger than in the wake of the shedding disc.

To further elucidate the evolution of these spectral peaks, especially downstream of the mesh disc, streamwise measurements were carried out for $0.5 \leqslant x/D \leqslant 40$ at the respective inner edges of the two discs in the M-S20 configuration ($y/D = -0.5$ and $y/D = 0.5$ for the M and S20 discs, respectively). The pre-multiplied spectrograms computed from these measurements are shown in figure 5. Downstream of the S20 disc, a spectral peak at 7.5 Hz (similar to the single disc measurement) is observed from $0.5D$. While the same peak is observed downstream of the M disc, it appears farther

https://doi.org/10.1017/jfm.2025.10799 Published online by Cambridge University Press

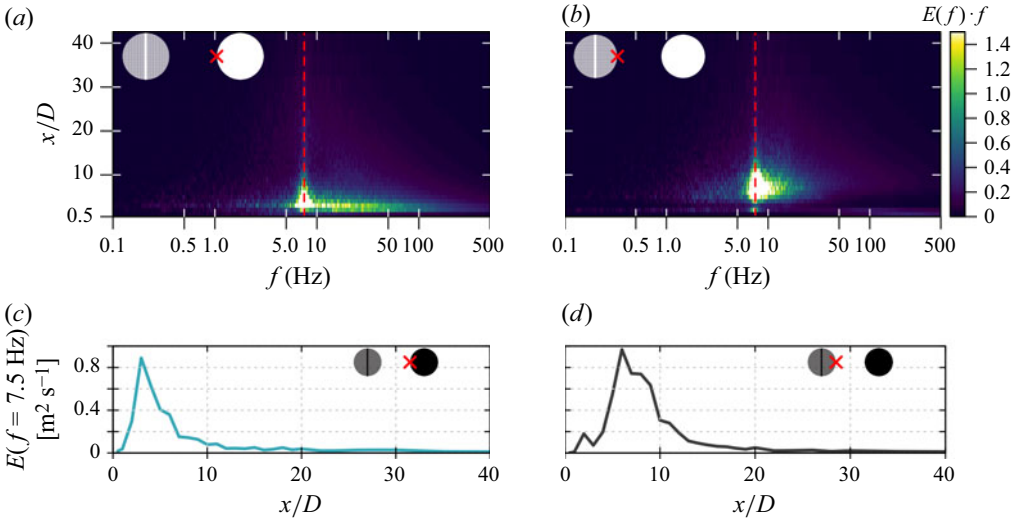


Figure 5. Downstream evolution of the pre-multiplied spectrograms measured at the edge of (*a*) the S20 disc and (*b*) the M disc for the M-S20 case; downstream evolution of the energy within the shedding peak, $E(f = 7.5\ \text{Hz})$, at the edge of (*c*) the S20 disc and (*d*) the M disc for the M-S20 case. The spanwise measurement positions are marked by the red crosses in the sketch.

downstream compared with the S20 disc's side of the wake. This becomes even clearer when comparing the one-dimensional slices of the downstream evolution of the energy within the spectral peak, $E(f = 7.5\ \text{Hz})$, for the S20 and M discs in figures 5(*c*) and 5(*d*), respectively. This suggests that the M disc is not the source of the periodicity and does not start shedding itself. Instead, the wake of the M disc picks up the oscillation of the S20 disc wake. This indicates that the strong velocity deficit wake of the mesh disc (cf. figure 3) is receptive to continuous periodic excitation from one side in the downstream direction.

5. Stability analysis

The mean velocity profile of the mesh disc is thinner and has a larger deficit, cf. figure 2(*a*), which amounts to higher velocity gradients compared with those of the solid discs. While the mesh disc's wake shows no dominant periodicity in isolation, it picks up the spectral signature of the solid discs when in proximity, as discussed in the previous section. These observations suggest that the mesh disc's wake is receptive to the fluctuations in the frequency band where the employed solid discs shed. To look into this further, linear stability analysis was carried out on the wake profiles of the single discs at $x/D_i = 8$. Specifically, stability analysis was performed on profiles obtained by fitting the modified eddy viscosity wake model (3.1) to the measured radial profiles of the mean streamwise velocity (dashed lines in figure 2*a*). The single disc cases are axisymmetric and the fluctuations of interest are those amplifying along the streamwise direction. Thus, the current case is treated as a one-dimensional spatial stability problem. The streamwise amplification rate of various fluctuations was obtained by solving the Rayleigh equation using the Chebyshev spectral collocation method (Weideman & Reddy 2000).

The streamwise amplification rates ($-\alpha_i$) of various fluctuations in the four investigated disc wakes are presented in figure 6. For the solid discs, the measured shedding frequency is close to the most unstable fluctuations from the respective stability computations. As

https://doi.org/10.1017/jfm.2025.10799 Published online by Cambridge University Press

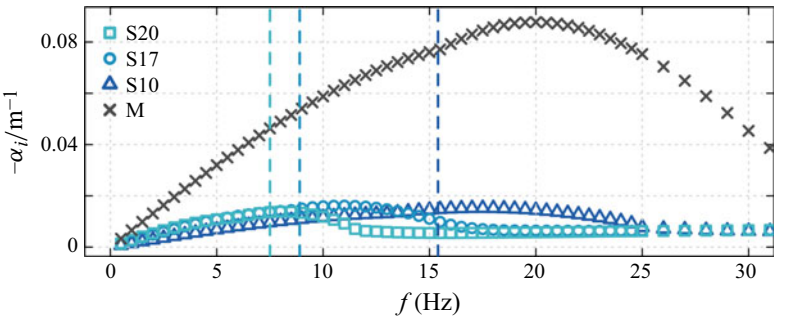


Figure 6. Linear stability analysis: amplification rate $-\alpha_i$ against frequency for the single wakes of the three solid discs and the M disc. The vertical lines mark the shedding frequencies of the respective solid discs.

hypothesised earlier, out of the four disc wakes investigated, the mesh disc's wake seems to be the most unstable in the solid discs' shedding frequency range. It is therefore highly receptive to external forcing at these frequencies. Thus, when in proximity to another disc that has a distinct spectral peak, it picks it up quite effortlessly.

It is worth noting that, while the stability analysis reveals the wake of the porous disc to be highly receptive to perturbations across a broad range of frequencies, this receptivity in the linear framework does not necessarily translate to self-sustained vortex shedding when the disc is in isolation, as confirmed by our experimental data. This apparent contradiction is attributed to the porosity of the M disc, whose solidity is lower than 75 %. Such geometric features are known to dampen instabilities and weaken recirculation zones (Castro 1971; Cicolin *et al.* 2024), which are critical for the onset of self-excited vortex shedding. Moreover, the porous M disc acts as a fine grid locally, producing small-scale turbulence which acts to homogenise the local flow, a process that also inhibits vortex shedding (Vinnes *et al.* 2023). In contrast, solid discs – despite exhibiting lower amplification rates – support stronger flow separation and recirculation zones, which facilitate sustained vortex shedding. The porous disc thus behaves as a passive amplifier, responding to external perturbations from adjacent shedding bodies rather than acting as an autonomous oscillator.

To connect these findings to real-life applications, linear stability analysis was exemplarily repeated on full-scale wind turbine wake profiles measured with light detection and ranging (LiDAR) by Zhan, Letizia & Iungo (2020) that are openly accessible (Iungo 2020). While wind turbines are not the exclusive use of this knowledge, they are a common example for which there is significant contemporary research and impact. We specifically consider profiles $5.25D_{wt}$ downstream of a 2.3 MW wind turbine with diameter $D_{wt} = 108$ m at an inflow velocity corresponding to 75 % of the rated wind speed, where the wind turbine operates at maximum thrust. Four profiles from Zhan *et al.* (2020) are plotted in figure 7(*a*), grouped by their atmospheric stability conditions: weakly convective (WC), neutral (NT), weakly stable (WS) and stable (ST), as characterised by the bulk Richardson number. Using far-wake assumptions (axisymmetry and the lack of rotor-specific structures (Toloui, Chamorro & Hong 2015; Stevens & Meneveau 2017)), fits from (3.1) are applied. In figure 7(*b*), the non-dimensionalised amplification rate $-\alpha_i D_i$ is plotted against the reduced frequency, $f D_i/U_\infty$. Here, we present the non-dimensionalised quantities as we compare the results from the wind turbine wakes and the results from the solid and M discs, which are orders of magnitude different in scale.

We find that the wake of this wind turbine is particularly receptive to excitations in the range $0.2 \lesssim f D_i/U_\infty \lesssim 0.25$, which corresponds to the reduced frequency band

https://doi.org/10.1017/jfm.2025.10799 Published online by Cambridge University Press

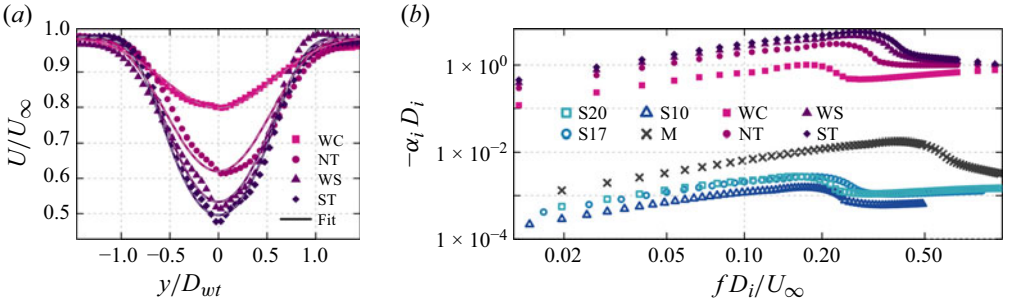


Figure 7. (*a*) Normalised mean velocity profiles from LiDAR measurements (from Iungo (2020)) $5.25D_{wt}$ downstream at different atmospheric stabilities (WC =; weakly convective; NT =; neutral; WS =; weakly stable; ST =; stable) with corresponding fits. (*b*) Linear stability analysis: non-dimensionalised amplification rate $-\alpha_i D_i$ over reduced frequency fD_i/U_∞ for the wind turbine wake profiles in comparison with the single wakes of the three solid discs and the M disc.

associated with wind turbine wake meandering reported in several previous studies (Medici & Alfredsson 2008; Chamorro *et al.* 2013; Okulov *et al.* 2014). The corresponding dimensional frequencies are $\approx 0.015-0.019$ Hz, a frequency band that is relevant in the atmospheric boundary layer (Morales, Wächter & Peinke 2012; Sim, Peinke & Maass 2023). This suggests that, if one turbine exhibits wake meandering, adjacent ones are likely to also adopt the same frequency in their wakes, and that frequency content inherent to the incoming boundary layer may initiate these processes. Our findings are therefore particularly relevant for wind farms.

6. Conclusions

Here, we investigated the interaction of two wakes with different intrinsic properties generated by two different disc types in a side-by-side setting: a 'dead' wake of a non-shedding porous disc, and oscillating wakes from shedding solid discs of varying diameters with different dimensional shedding frequencies. For all cases, we observe that the spectrum in the wake of the non-shedding disc displays a peak at the shedding frequency of the adjacent solid disc.

As the wake of the porous disc adopts different shedding frequencies from the three solid discs, and given additional measurements showing that the onset of the spectral peak occurs farther downstream than for the solid discs, we conclude that this peak does not originate from induced shedding of the porous disc. Instead, the 'dead' wake of the porous disc is animated by the periodic oscillations present in the wake of the solid discs and begins to oscillate accordingly. Linear stability analysis confirms the high receptivity of the porous disc's wake to frequencies particularly around 20 Hz, and we exemplarily indicate the importance of these results for real-life applications by demonstrating that high receptivity can be expected in wind turbine wakes for reduced frequencies in the range $0.2-0.25$.

Acknowledgements. We thank M. Obligado for several insightful conversations on wake interactions. We also thank T. Kolbjørnsen for assisting with the measurements.

Declaration of interests. The authors report no conflict of interest.

Author contributions. IN: Conceptualisation; Methodology; Formal analysis; Visualisation; Writing: original draft and review & editing; Data curation. SY: Writing: original draft and review & editing; Formal analysis. RJH: Conceptualisation; Writing: review & editing; Supervision; Funding acquisition.

https://doi.org/10.1017/jfm.2025.10799 Published online by Cambridge University Press

Data availability statement. The data that support the findings of this article are openly available at https://doi.org/10.18710/RC8LFD, cf. Neunaber *et al.* (2025).

References

Aubrun, S. 2019 Round-robin tests of porous disc models. *J. Phys. Conf. Ser.* **1256**, 012004.

Baj, P. & Buxton, O.R.H. 2017 Interscale energy transfer in the merger of wakes of a multiscale array of rectangular cylinders. *Phys. Rev. Fluids* **2**, 114607.

Bastankhah, M., Welch, B.L., Martínez-Tossas, L.A., King, J. & Fleming, P. 2021 Analytical solution for the cumulative wake of wind turbines in wind farms. *J. Fluid Mech.* **911**, A53.

Benedict, L. & Gould, R. 1996 Towards better uncertainty estimates for turbulence statistics. *Exp. Fluids* **22**, 129–136.

Berstad, F.O.J., Hearst, R.J. & Neunaber, I. 2025 Wake merging and turbulence transition downstream of side-by-side porous discs. *J. Fluid Mech.* **1015**, A39.

Bourhis, M. & Buxton, O.R.H. 2024 Influence of freestream turbulence and porosity on porous disk-generated wakes. *Phys. Rev. Fluids* **9**, 124501.

Brown, G.L. & Roshko, A. 2012 Turbulent shear layers and wakes. *J. Turb.* **13**, N51.

Cafiero, G., Obligado, M. & Vassilicos, J.C. 2020 Length scales in turbulent free shear flows. *J. Turbul.* **21** (4), 243–257.

Castro, I.P. 1971 Wake characteristics of two-dimensional perforated plates normal to an air-stream. *J. Fluid Mech.* **46** (3), 599–609.

Nedić, J., Vassilicos, J.C. & Ganapathisubramani, B. 2013 Axisymmetric turbulent wakes with new nonequilibrium similarity scalings. *Phys. Rev. Lett.* **111**, 144503.

Chamorro, L.P., Hill, C., Morton, S., Ellis, C., Arndt, R.E.A. & Sotiropoulos, F. 2013 On the interaction between a turbulent open channel flow and an axial-flow turbine. *J. Fluid Mech.* **716**, 658–670.

Cicolin, M.M., Buxton, O.R.H., Assi, G.R.S. & Bearman, P.W. 2021 The role of separation on the forces acting on a circular cylinder with a control rod. *J. Fluid Mech.* **915**, A33.

Cicolin, M.M., Chellini, S., Usherwood, B., Ganapathisubramani, B. & Castro, I.P. 2024 Vortex shedding behind porous flat plates normal to the flow. *J. Fluid Mech.* **985**, A40.

Dadmarzi, F.H., Narasimhamurthy, V.D., Andersson, H.I. & Pettersen, B. 2018 Turbulent wake behind side-by-side flat plates: computational study of interference effects. *J. Fluid Mech.* **855**, 1040–1073.

Hegazy, A., Blondel, F., Cathelain, M. & Aubrun, S. 2022 LiDAR and SCADA data processing for interacting wind turbine wakes with comparison to analytical wake models. *Renew. Energy* **181**, 457–471.

Hertwig, D., Gough, H.L., Grimmond, S., Barlow, J.F., Kent, C.W., Lin, W.E., Robins, A.G. & Hayden, P. 2019 Wake characteristics of tall buildings in a realistic urban canopy. *Boundary-Layer Meteorol.* **172** (2), 239–270.

Hultmark, M. & Smits, A.J. 2010 Temperature corrections for constant temperature and constant current hot-wire anemometers. *Meas. Sci. Technol.* **21**, 105404.

Hölling, M. *et al.* 2025 Round-Robin test II – wake measurements of porous discs under clearly defined boundary conditions. *J. Phys. Conf. Ser.* **3016** (1), 012013.

Iungo, G.V. 2020 LiDAR cluster statistic of wind turbine wakes [data set]. In *Wind Energy*. Zenodo.

Kleine, V.G., Franceschini, L., Carmo, B.S., Hanifi, A. & Henningson, D.S. 2022 The stability of wakes of floating wind turbines. *Phys. Fluids* **34** (7), 074106.

Martínez-Tossas, L.A., Branlard, E., Shaler, K., Vijayakumar, G., Ananthan, S., Sakievich, P. & Jonkman, J. 2022 Numerical investigation of wind turbine wakes under high thrust coefficient. *Wind Energy* **25** (4), 605–617.

Maus, J., Peinke, J. & Hölling, M. 2022 Experimental investigation on the effect of lateral turbine spacing on interactions of wakes. *J. Phys. Conf. Ser.* **2265** (4), 042064.

Medici, D. & Alfredsson, P.H. 2008 Measurements behind model wind turbines: further evidence of wake meandering. *Wind Energy* **11** (2), 211–217.

Messmer, T., Hölling, M. & Peinke, J. 2024 Enhanced recovery caused by nonlinear dynamics in the wake of a floating offshore wind turbine. *J. Fluid Mech.* **984**, A66.

Miau, J.J., Leu, T.S., Liu, T.W. & Chou, J.H. 1997 On vortex shedding behind a circular disk. *Exp. Fluids* **13**, 225–233.

Morales, A., Wächter, M. & Peinke, J. 2012 Characterization of wind turbulence by higher-order statistics. *Wind Energy* **15** (3), 391–406.

Neunaber, I., Yadala, S., Kolbjørnsen, T. & Hearst, R.J. 2025 Replication data for: Indiced periodicity in wakes.

Obligado, M., Klein, S. & Vassilicos, J.C. 2022 Interaction of two axisymmetric turbulent wakes. *Phys. Rev. Fluids* **7**, 114606.

https://doi.org/10.1017/jfm.2025.10799 Published online by Cambridge University Press

OKULOV, V.L., NAUMOV, I.V., MIKKELSEN, R.F., KABARDIN, I.K. & SØRENSEN, J.N. 2014 A regular Strouhal number for large-scale instability in the far wake of a rotor. *J. Fluid Mech.* **747**, 369–380.

PORTÉ-AGEL, F., BASTANKHAH, M. & SHAMSODDIN, S. 2020 Wind-turbine and wind-farm flows: a review. *Boundary-Layer Meteorol.* **174**, 1–59.

SATO, H. & OKADA, O. 1966 The stability and transition of an axisymmetric wake. *J. Fluid Mech.* **26** (2), 237–253.

SCOTT, R., VIGGIANO, B., DIB, T., ALI, N., HÖLLING, M., PEINKE, J. & CAL, R.B. 2020 Turbine partial wake merging description and quantification. *Wind Energy* **23** (7), 1610–1618.

SIM, S.K., PEINKE, J. & MAASS, P. 2023 Signatures of geostrophic turbulence in power spectra and third-order structure function of offshore wind speed fluctuations. *Sci. Rep.* **13** (13411).

SONG, Y., TI, Z., LI, Y., YOU, H. & ZHU, J. 2024 Modelling of wake-induced vibration of a long-span bridge with separated parallel nonidentical decks. *Structures* **69**, 107427.

STEIROS, K., OBLIGADO, M., BRAGANÇA, P., CUVIER, C. & VASSILICOS, J.C. 2025 Turbulent shear flow without vortex shedding, Reynolds shear stress and small-scale intermittency. *J. Fluid Mech.* **1002**, A51.

STEVENS, R.J.A.M. & MENEVEAU, C. 2017 Flow structure and turbulence in wind farms. *Annu. Rev. Fluid Mech.* **49** (2017), 311–339.

TOLOUI, M., CHAMORRO, L.P. & HONG, J. 2015 Detection of tip-vortex signatures behind a 2.5MW wind turbine. *J. Wind Eng. Ind. Aerod.* **143**, 105–112.

VINNES, M.K., GAMBUZZA, S., GANAPATHISUBRAMANI, B. & HEARST, R.J. 2022 The far wake of porous disks and a model wind turbine: similarities and differences assessed by hot-wire anemometry. *J. Renew. Sustain. Ener.* **14** (2), 023304.

VINNES, M.K., NEUNABER, I., LYKKE, H.-M.H. & HEARST, R.J. 2023 Characterizing porous disk wakes in different turbulent inflow conditions with higher-order statistics. *Exp. Fluids* **64** (2), 25.

WEIDEMAN, J.A. & REDDY, S.C. 2000 A MATLAB differentiation matrix suite. *ACM Trans. Math. Software* **26** (4), 465–519.

WONG, C.W., ZHOU, Y., ALAM, M.M. & ZHOU, T.M. 2014 Dependence of flow classification on the Reynolds number for a two-cylinder wake. *J. Fluid. Struct.* **49**, 485–497.

ZHAN, L., LETIZIA, S. & IUNGO, G.V. 2020 LiDAR measurements for an onshore wind farm: wake variability for different incoming wind speeds and atmospheric stability regimes. *Wind Energy* **23** (3), 501–527.

ZHOU, Y. & ALAM, M.M. 2016 Wake of two interacting circular cylinders: a review. *Int. J. Heat Fluid Fl.* **62**, 510–537.

https://doi.org/10.1017/jfm.2025.10799 Published online by Cambridge University Press